Title
Effects of toroidal rotation shear on toroidicity-induced Alfvén eigenmodes in the National Spherical Torus Experiment

Journal
Physics of Plasmas, 17(12)

ISSN
1070-664X

Authors
Podestà, M
Bell, RE
Fredrickson, ED
et al.

Publication Date
2010-12-01

DOI
10.1063/1.3524288

Effects of toroidal rotation shear on toroidicity-induced Alfvén eigenmodes in the National Spherical Torus Experiment

M. Podestà,[1] R. E. Bell,[1] E. D. Fredrickson,[1] N. N. Gorelenkov,[1] B. P. LeBlanc,[1] W. W. Heidbrink,[2] N. A. Crocker,[3] S. Kubota,[3] and H. Yuh[4]
[1]*Princeton Plasma Physics Laboratory, Princeton, New Jersey 08543, USA*
[2]*University of California, Irvine, California 92697, USA*
[3]*University of California, Los Angeles, California 90095, USA*
[4]*Nova Photonics, Princeton, New Jersey 08543, USA*

(Received 23 August 2010; accepted 15 November 2010; published online 7 December 2010)

The effects of a sheared toroidal rotation on the dynamics of bursting toroidicity-induced Alfvén eigenmodes are investigated in neutral beam heated plasmas on the National Spherical Torus Experiment (NSTX) [M. Ono *et al.*, Nucl. Fusion **40**, 557 (2000)]. The modes have a global character, extending over most of the minor radius. A toroidal rotation shear layer is measured at the location of maximum drive for the modes. Contrary to results from other devices, no clear evidence of decorrelation of the modes by the sheared rotation is found. Instead, experiments with simultaneous neutral beam and radio-frequency auxiliary heating show a strong correlation between the dynamics of the modes and the instability drive. It is argued that kinetic effects involving changes in the mode drive and damping mechanisms other than rotation shear, such as continuum damping, are mostly responsible for the bursting dynamics of the modes on NSTX.
 [doi:10.1063/1.3524288]

I. INTRODUCTION

Waves in the Alfvén frequency range can interact with a fast-ion population, leading to loss or redistribution of fast particles.[1,2] In particular, the nonlinear evolution following saturation of multiple modes may lead to their strong coupling and, eventually, to the overlap of mode resonances in phase space.[3,4] As a result, extended regions of the fast ion distribution function can provide free energy to further sustain the growth of the modes. These phase space (or *kinetic*) effects may be responsible for the variety of phenomena observed in experiments on toroidicity-induced Alfvén eigenmodes (TAEs). A single mode can split into multiple frequencies[5] or show a series of frequency *chirps*. The latter can result in a rapid increase as well as a decrease of the observed mode frequency.[6] The *stochastization* of fast ion phase space associated with chirping modes is thought to be responsible for the enhanced losses and redistribution of fast ions observed experimentally.[7–9] Clear signatures of nonlinear TAE behavior and induced fast ion losses are commonly observed in neutral beam (NB) heated plasmas on the National Spherical Torus Experiment (NSTX),[10] where NB injection provides the main source of additional heating and momentum.

Understanding the mechanisms leading to strongly nonlinear mode dynamics, including mode-mode coupling, is of broad interest for the design of future fusion devices. Indeed, it represents the first step for designing specific tools to reduce, or even suppress, the deleterious loss of fast ions associated with bursting TAE activity. Experimental results from large aspect ratio tokamaks suggest that a sheared toroidal flow may represent a possible suppression mechanism. Sufficiently strong gradients in the toroidal rotation would cause a radial decorrelation of the TAE mode structure, thus reducing the saturation level and clamping the growth rate. On JET, an increase in the damping rate of global TAE modes with toroidal mode number $n=1$ was observed for increasing values of the rotation shear at high (>6.5 MW) injected NB power.[11] No clear trend was observed for lower injected power. The damping rate of the stable modes was directly measured through synchronous detection of the perturbations driven through the JET saddle coils.[12] Similar results, but for unstable TAEs, have been reported from JT60-U for intermediate-n modes.[13] In this case, both NB and rf injection were used to affect the rotation profile and the fast ion drive of the modes. The decrease in the TAE activity was associated with the enhanced rotation shear caused by counter-NB injection. For both devices, the predictions from stability analysis indicated that damping mechanisms such as ion/electron Landau damping and radiative damping are too small to explain the experimental results. According to theory, a decorrelation mechanism analogous to that provided by toroidal rotation shear could be provided by sheared *poloidal* flows, such as the self-generated $\mathbf{E}\times\mathbf{B}$ flow induced by the Reynold stress associated with TAE turbulence.[14] The study of the effects of poloidal rotation and turbulence on TAEs is beyond the scope of this paper and is not considered in the following.

In this paper, the study of rotation shear effects on the dynamics of TAEs is extended to NB-heated plasmas of the spherical torus NSTX. The peculiarities of spherical torii[15,16] lead to a considerably different environment for TAE studies with respect to conventional tokamaks. For instance, the small aspect ratio and the large edge safety factor lead to radially extended, *global* modes composed by a large number of poloidal harmonics. Because of the large rotation frequency and magnetic shear, strong distortions of the Alfvén

continuum, hence of the mode structure,[17] can be expected with respect to large aspect ratio devices.[18] Furthermore, the contribution of the fast ion pressure to the total plasma β (ratio of plasma to magnetic pressure) can be $O(50\%)$, thus providing a large drive for the modes. All these features make NSTX a suitable environment to study Alfvénic modes and to provide data to challenge and validate theories and numerical codes.

The mode dynamics observed on NSTX include the evolution from a quasistationary phase into a regime characterized by dramatic frequency and amplitude bursts, the so-called TAE *avalanches*.[8,19] The primary interest for the present study is an intermediate phase, prodromic to the avalanching regime causing fast ion losses, during which relatively small amplitude and frequency changes compared to avalanches are observed. If a sheared flow can directly affect the TAE evolution during this early phase, new avenues may open up for controlling the TAE dynamics, thus limiting the detrimental effect of avalanches on fast ion confinement. Testing this hypothesis and complementing the previous studies on mechanisms for TAE stabilization with results from a low aspect ratio configuration are the primary goals of this work.

The paper is organized as follows. The NSTX plasmas studied in this work and the general observations on TAE dynamics are described in Sec. II. Section III presents the measurements of toroidal rotation and its relationship with other quantities, such as the fast ion profile. The effects of rotation shear are discussed in Sec. IV. The lack of clear experimental evidence of mode suppression by rotation shear motivates the extension of the study to the TAE drive (Sec. V). Section VI summarizes the main results and concludes the paper.

II. EXPERIMENTAL SCENARIO

NSTX is a small aspect ratio device, with major and minor radii $R_0=0.9$ m and $a=0.65$ m (aspect ratio $R_0/a \approx 1.3$). For the experiments discussed herein, the magnetic field is 5.5 kG. The plasma current is 700–900 kA for a pulse duration of ~0.6 s. L-mode deuterium plasmas are mainly investigated. Density and temperature are $n_e \approx 3\times10^{19}$ m^{-3} and $T_i \approx T_e \leq 1.5$ keV (subscripts e, i refer to electrons and ions, respectively), see Fig. 1(b). Electron and ion plasma parameters, including rotation, are measured by a Thomson scattering[20] and a charge-exchange recombination spectroscopy system.[21] The difference between the measured carbon velocity and the main ion velocity,[22] which determines the Doppler shift of the TAE frequencies, has been estimated from other studies to be <5% (Ref. 23) and is negligible for the purposes of this study. The total plasma β (ratio of plasma to magnetic energy) is $\lesssim$15%. Up to 3 MW of NB power is injected from three sources with tangency radii of 69, 59, and 49 cm. The maximum acceleration voltage is 90 kV. The injected species is deuterium. The velocity of fast ions resulting from charge-exchange of the injected neutrals is up to five times the Alfvén velocity. Several resonances with the fast ion population can thus destabilize waves in the Alfvén frequency range, including TAEs, as commonly

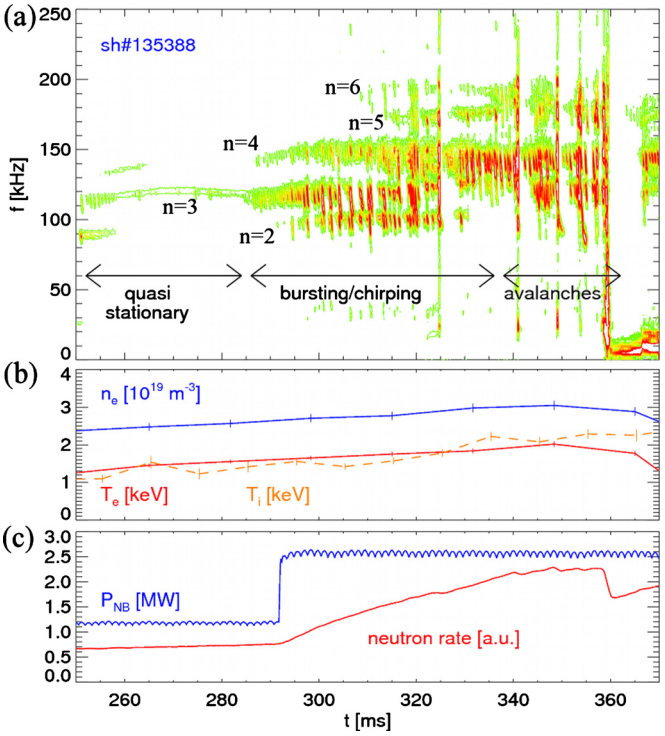

FIG. 1. (Color online) (a) Spectrogram showing TAE activity in the range $f=70-200$ kHz for discharge 135388. (b) Temporal evolution of the central electron density and electron and ion temperature (ion temperature is averaged over 95–105 cm). (c) Waveforms of NB power and neutron rate. Note the drop of the neutron rate at $t \approx 360$ ms, corresponding to an avalanche, which indicates a loss of fast ions from the core plasma.

observed.[7] In addition to neutral beams, a high-harmonic fast wave (HHFW) system[24] is used to heat the plasma with $P_{rf}=2$ MW.

Figure 1(a) illustrates a spectrogram from Mirnov coils measuring magnetic field fluctuations close to the low-field side vacuum vessel wall. Multiple modes are visible in the frequency range 70–200 kHz. The modes are first destabilized during the current ramp-up ($t \leq 200$ ms). In this initial stage they are identified as reverse-shear Alfvén eigenmodes (RSAEs).[25] After the beginning of the current flat-top RSAEs gradually evolve into TAEs, driven unstable by the injected beam ions.[9] No direct measurement of the safety factor profile $q(R,t)$ is available for this discharge in the time window $t=240-400$ ms. A reconstruction of the average $q(R,t)$ has been performed through the Grad–Shafranov equilibrium reconstruction code LRDFIT (Ref. 26) by varying the NB timing on a shot-to-shot basis. The analysis shows that the discharges under investigation have a reversed-shear q profile with $q_{min} \sim 2$ at $t \sim 300$ ms. Toroidal mode numbers are $n=2-8$. The dominant modes have $n=2-4$ and a frequency in the laboratory frame $f \approx 90-150$ kHz. The toroidal rotation frequency, causing the Doppler shift between the mode frequency in the plasma and laboratory frames, is typically 15–30 kHz on the magnetic axis. As the discharge evolves, the fast ion content gradually builds up, as seen from fast ion density measurements (see Sec. III). The modes exhibit a quasistationary behavior, then their dynamic becomes more turbulent. Although in some discharges the transition occurs

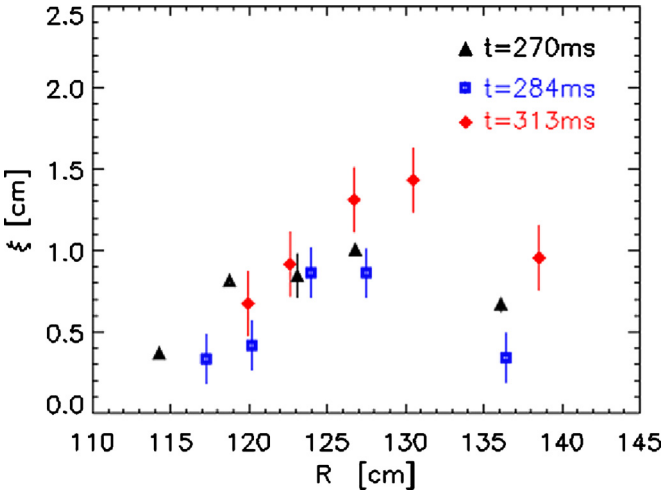

FIG. 2. (Color online) Radial displacement associated with a $n=3$ mode, measured by a multichannel reflectometer at three different times for the discharge in Fig. 1.

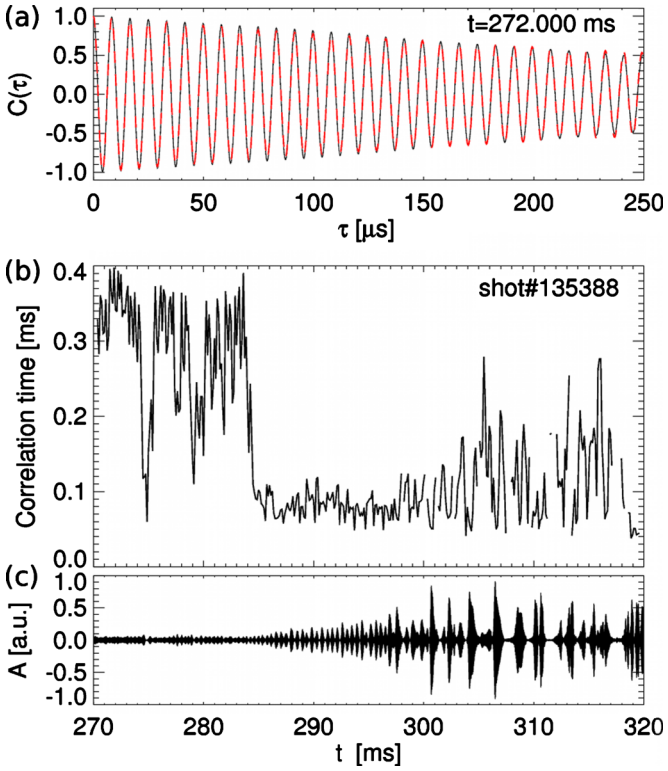

FIG. 3. (Color online) (a) Example of fit of the autocorrelation function as a function of the time lag to infer the autocorrelation time τ_{corr}. The experimental data (solid) and the result of the fit (dashed) are shown. (b) Autocorrelation time for the dominant $n=3$ mode, calculated by windowing the filtered signal (bandpass, 105–130 kHz range) in subsamples with duration of 1 ms. Note the drop in the autocorrelation after ≈285 ms, corresponding to the onset of the bursting/chirping regime. (c) Filtered signal from a Mirnov coil, showing the beginning of amplitude bursts at $t\approx285$ ms.

without a change in the injected NB power, a bursty regime is indeed favored by turning on a second NB source. After $t\approx290$ ms relatively large excursions in both amplitude and frequency are measured, eventually ending up with a dramatic burst of TAE activity. The latter is dubbed *avalanche* and may result in a drop in the neutron rate of up to 30%,[8,9] see Fig. 1(c). Depending on the frequency and amplitude variation modes are classified as *quasistationary*, *bursting/chirping*, or *avalanching*. Although somewhat arbitrary, this classification provides a practical tool for the following discussion. Note that only downchirping TAE modes are observed here, contrary to other experiments from which both upward and downward frequency sweeps have been reported.[6,27]

The mode structure, measured by a multichannel reflectometer system,[25] extends over a good fraction of the minor radius (Fig. 2) up to $R\approx140$ cm, with maximum amplitude at $R=120-130$ cm. For reference, the magnetic axis and the last closed flux surface are at $R\sim103$ cm and $R\sim145$ cm. The mode evolution described above is representative of discharges spanning a broad range of plasma parameters with $P_{NB}\leq3$ MW in both helium and deuterium plasmas.

The transition of the dominant $n=3$ mode from quasistationary to bursting/chirping illustrated in Fig. 1 can be quantified through the autocorrelation time of magnetic fluctuations, τ_{corr}, as a function of time (Fig. 3). τ_{corr} is calculated by fitting the autocorrelation function $C(\tau)=k_{norm}\int_{-\infty}^{+\infty}s(t)s(t-\tau)dt$ as a function of the time lag. In practice, $C(\tau)\approx\cos(2\pi f_{mode}\tau)\times\exp(-|\tau|/\tau_{corr})$, see Fig. 3(a). $s(t)$ is the measured signal, filtered around the mode frequency f_{mode} for a specific n, and k_{norm} a normalization factor, such that $C(\tau=0)\equiv1$. $C(\tau)$ is calculated over a moving window of 1 ms. A clear transition is observed as the mode develops bursting/chirping features after approximately $t=285$ ms. Typical values before that time are $\tau_{corr}\lesssim0.4$ ms, indicating that the oscillation remains coherent over ~50 wave cycles. After the transition has occurred, τ_{corr} drops to ~0.1 ms. This can be explained by decomposing τ_{corr} as $\tau_{corr}^{-1}=\tau_{phase}^{-1}+\tau_{freq}^{-1}$, where the two terms represent the decorrelation time associated with phase and frequency variations of the mode, respectively. As the frequency undergoes a rapid change, $\tau_{corr}\approx\tau_{freq}$ is primarily determined by the typical frequency chirp rate. The transition between quasistationary and bursting/chirping regimes, as seen in $C(\tau)$, occurs in ≈2 ms. This is much shorter than the time-scales associated with changes in the background plasma profiles (e.g., density, temperature, rotation, or safety factor profile), beam ions slowing down, and scattering (approximately tens of milliseconds).

To investigate in more detail the TAE dynamics, we focus in the following on the time window of 260–390 ms, when TAEs show an almost constant frequency separation between peaks with consecutive n's. This suggests that the modes have a common frequency in the plasma frame f_0^{TAE}, such that[28]

$$f_{lab,n}^{TAE}=f_0^{TAE}+nf_{Doppler}^{TAE}, \quad (1)$$

where $f_{lab,n}^{TAE}$ is the frequency for the toroidal mode number n as measured in the laboratory frame and $f_{Doppler}^{TAE}$ the Doppler shift caused by plasma rotation. Diamagnetic corrections to $f_{Doppler}^{TAE}$ are estimated to be $\lesssim1$ kHz and are neglected here, as well as the differential rotation between impurity and main ions.[22] In practice, a Gaussian fit of the peaks in the fast Fourier transform (FFT) spectra from 1.25 ms time windows

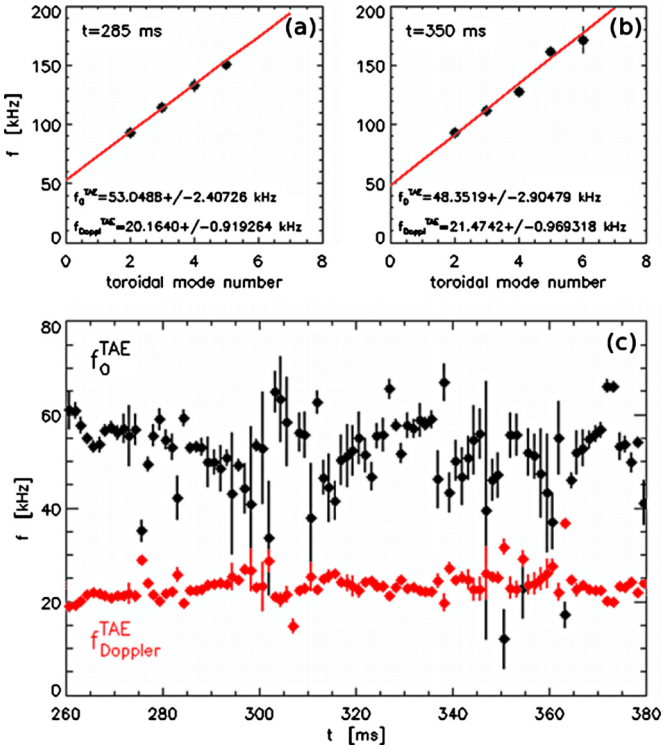

FIG. 4. (Color online) [(a) and (b)] Fit of the peak frequency vs toroidal mode number based on Eq. (1) for modes with $n=2-6$. The two different times correspond to the beginning of weakly bursting activity and to strong bursts. The peak frequency and its spread (indicated by the vertical bar) are obtained from a Gaussian fit of the FFT spectrum obtained from a moving time window of 1.25 ms. (c) Time history of the reconstructed mode frequency in the plasma frame, f_0^{TAE}, and TAE Doppler shift frequency, $f_{\mathrm{Doppler}}^{\mathrm{TAE}}$.

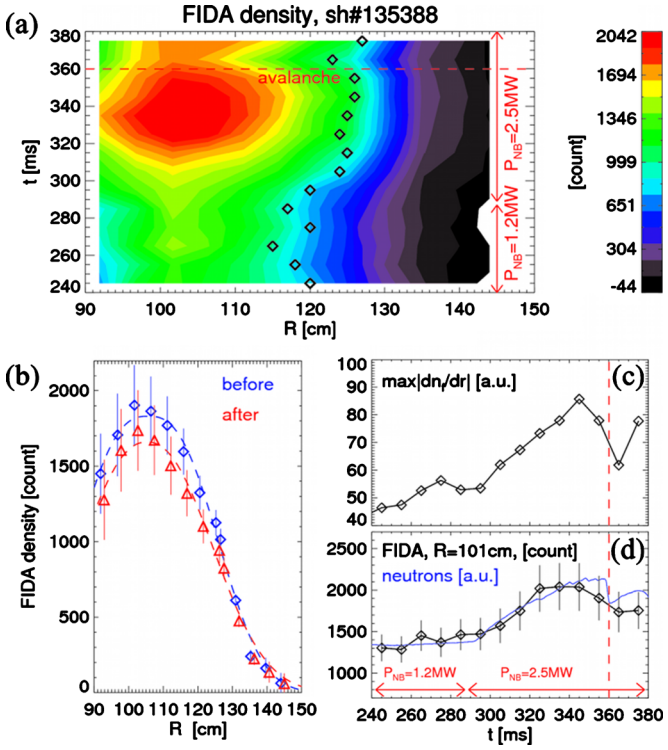

FIG. 5. (Color online) (a) Fast ion density evolution measured by FIDA. Diamonds indicate the radius where the steepest fast ion density gradient is measured. (b) FIDA measurements from the central chord (diamonds, $R=101$ cm) compared to the neutron rate (thin, solid line). The latter is renormalized to highlight the similarity with the FIDA data. Both signals decrease after the large avalanche at $t\approx 360$ ms, indicated by the dashed vertical line. (c) Evolution of the steepest fast ion density gradient. (d) FIDA profiles before (diamonds) and after (triangles) the TAE avalanche at $t\approx 360$ ms.

is first used to determine the center frequency and frequency spread of the different modes. Then, a linear fit based on Eq. (1) provides the values of f_0^{TAE} and $f_{\mathrm{Doppler}}^{\mathrm{TAE}}$, see Figs. 4(a) and 4(b). The results as a function of time are reported in Fig. 4(c). The calculated Doppler shift is remarkably constant in time. f_0^{TAE} does not change substantially for $t\lesssim 290$ ms, corresponding to a phase with only one NB source.

Interestingly, Eq. (1) represents well the frequency behavior over time scales $\gtrsim 1$ ms. The mechanisms through which the different TAEs lock on a similar frequency are not yet clear. In principle, modes with different n can be destabilized by wave-particle resonances at different frequencies (cf. Ref. 9 and Fig. 14) and at different locations along the plasma minor radius. At present, it can be excluded that the modes are harmonics of a fundamental TAE mode or that they couple to each other through a stationary low frequency mode, as was observed in Ref. 28. The submillisecond dynamics is more complex, with each mode chirping independently of the others except for the largest bursts. The detailed analyses of fast frequency evolution and of the differentiation in time scales, which suggests that mode-mode coupling is at play for large amplitude bursts, are deferred to a separate publication.

By knowing the TAE Doppler shift frequency and the rotation profile, the radius at which they match each other is easily calculated and can be compared, for example, with the location of maximum TAE drive. The comparison makes more meaningful the study of the possible decorrelation mechanisms, as discussed in Sec. III.

III. ROTATION SHEAR EVOLUTION

Several quantities can affect the drive and evolution of TAEs. Here we focus on (i) the fast ion profile and its radial gradient and (ii) the toroidal rotation profile f_{rot} and its radial shear, $\propto \partial f_{\mathrm{rot}}/\partial R$. The fast ion density is measured on NSTX by a fast ion D-alpha (FIDA) diagnostic based on active charge-exchange recombination spectroscopy.[29] For the discharge under investigation, the fast ion content increases considerably as the second NB source is turned on at 290 ms [Figs. 5(a) and 5(b)]. At the same time, the gradient on the low-field side steepens up [Fig. 5(c)]. This correlates with an increase of activity in the TAE frequency range, consistent with the picture that the observed TAEs are driven unstable by the radial gradient of the fast ion profile. The fast ion density decreases after the avalanche at ≈ 360 ms [Fig. 5(d)], which causes a relaxation of the gradient.[8]

Since NB injection also represents the main source of torque, the fast ion profile evolution correlates with the plasma rotation in many aspects. Figure 6 shows the measured evolution of the toroidal rotation profile and its shear for the discharge illustrated in Fig. 1. The rotation profile peaks on axis and gradually increases to ~ 30 kHz after the

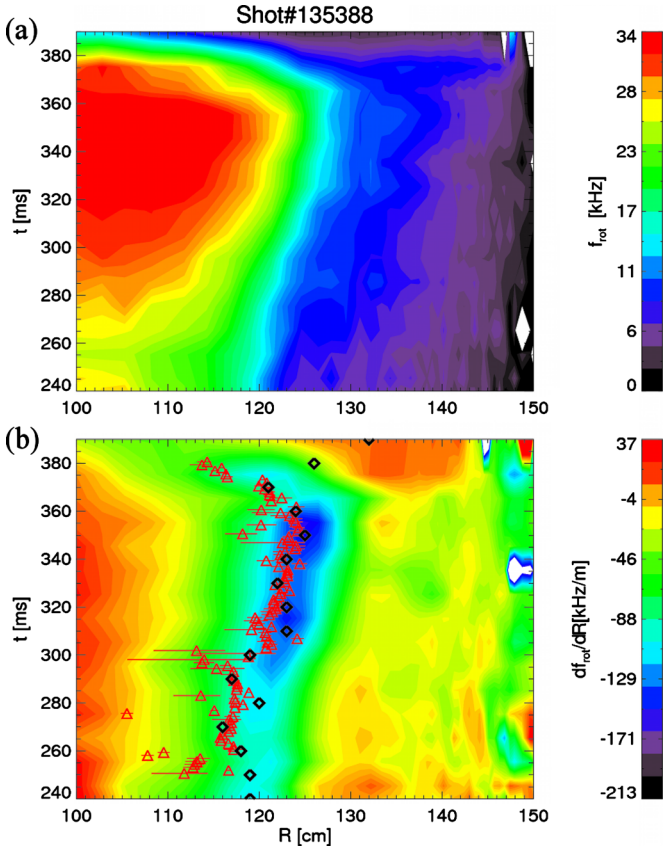

FIG. 6. (Color online) (a) Temporal evolution of the profiles of toroidal rotation frequency. (b) Radial shear of the rotation frequency, calculated as the radial gradient. The magnetic axis is at $R \approx 100$ cm. Triangles indicate the radius at which the plasma rotation frequency equals the Doppler shift frequency estimated from the modes, cf. Fig. 4. Diamonds show the position of steepest gradient of the fast ion profile on the low-field side.

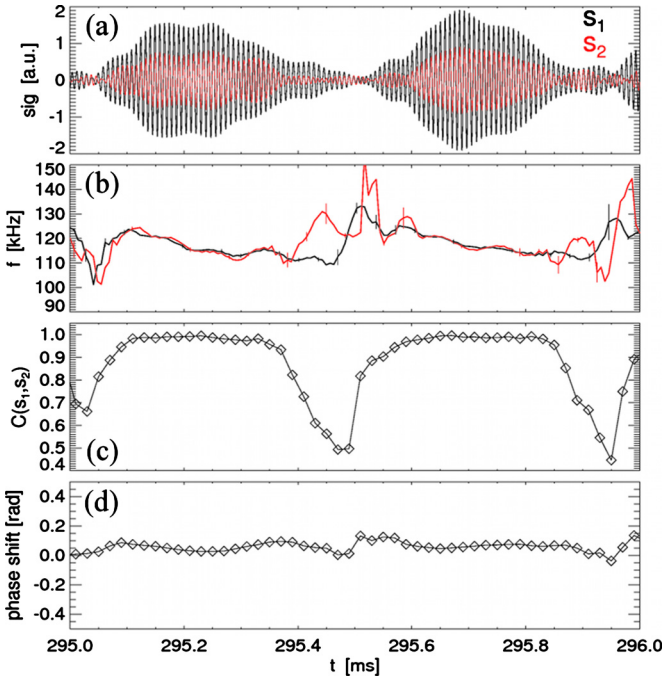

FIG. 7. (Color online) Correlation analysis of two reflectometer channels displaced by ~8 cm across the shear layer. (a) Raw signals associated with the $n=3$ mode measured at 117 cm (s_2) and 125 cm (s_1). (b) Frequency evolution for the two channels, reconstructed from the band-pass filtered signals. (c) Cross-correlation between the two signals. (d) Cross-phase reconstructed from the time-shift between raw signals.

second NB source is added. At the same time the profile broadens. The position of maximum radial shear, here defined as the radial gradient of the rotation profile, shifts outward from $R \approx 120$ cm to $R \approx 125$ cm [Fig. 6(b)]. The shear increases in time and a broader spatial region is affected by relatively large values.

The radius at which the plasma rotation matches the estimated Doppler shift frequency of the modes can be calculated from the measured rotation profile. This is illustrated in Fig. 6(b), along with the position of steepest fast ion gradient. A first observation is that the radii where $f_{\mathrm{rot}}=f_{\mathrm{Doppler}}^{\mathrm{TAE}}$ and of the steepest fast ion gradient are approximately equal and track each other in time. Second, the same position also corresponds to the location of largest rotation shear. A qualitative explanation implies that the fast ion profile resulting from NB injection determines at the same time the TAE driving term (through its gradient) and the toroidal rotation profile. This double role of the fast ion population means that the TAE modes naturally sit around the region of maximum velocity shear, thus favoring a competition between driving and decorrelating mechanisms. These observations, along with results from previous studies,[11,13] indicate that effects of rotation shear on the TAE modes might be expected.

For instabilities which are convected by a background flow, an upper limit for the decorrelation (or shearing) rate τ_{dec}^{-1} caused by a shear layer located at $R \approx R_{\mathrm{mode}}$ can be calculated from the toroidal velocity profile and the parallel wave number. τ_{dec} represents the minimum time required to

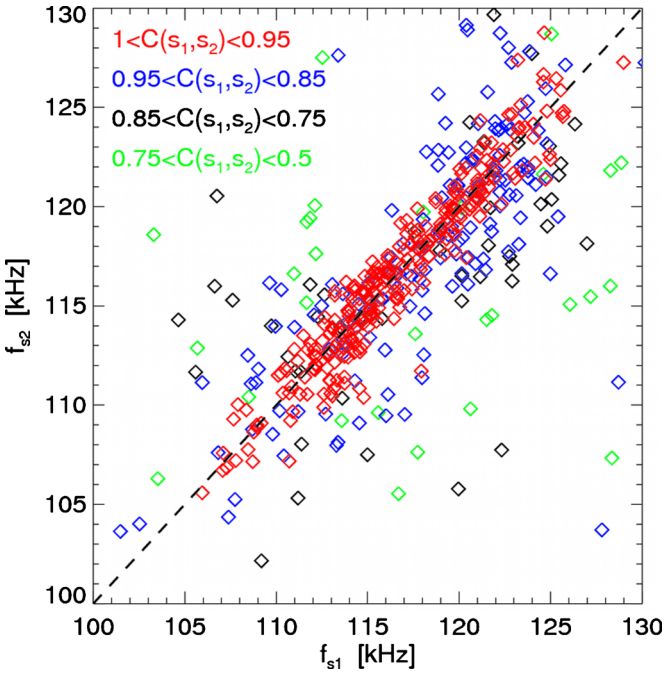

FIG. 8. (Color online) Frequency of the $n=3$ mode calculated from two reflectometer channels [cf. Fig. 7(b)] for discharge no. 135388, showing no systematic difference across the shear layer.

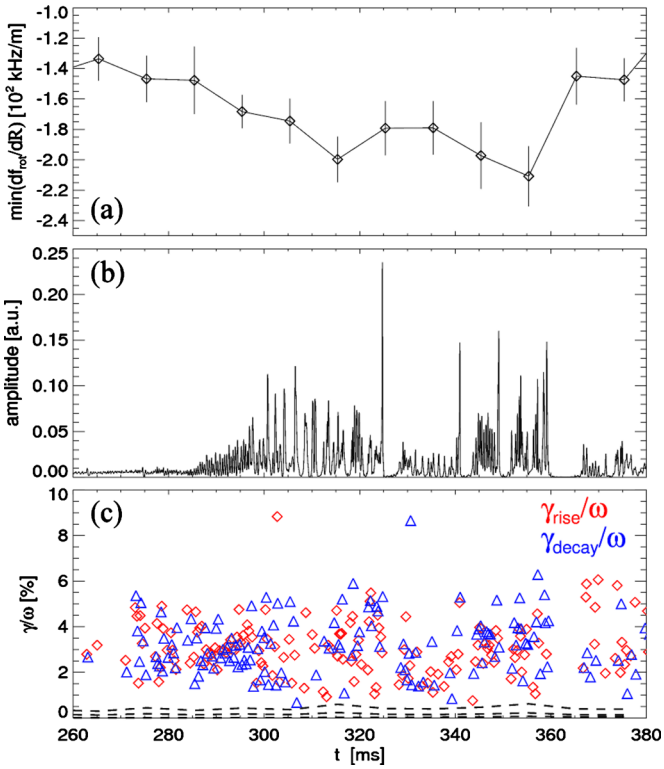

FIG. 9. (Color online) (a) Evolution of the maximum rotation shear. (b) rms mode amplitude for the $n=3$ mode in Fig. 1. (c) Amplitude rise (diamonds) and decay (triangles) rates normalized to the mode frequency, estimated from an exponential fit of the rising/decaying part of TAE bursts. The dashed lines show the decorrelation rate from rotation shear calculated through Eq. (2).

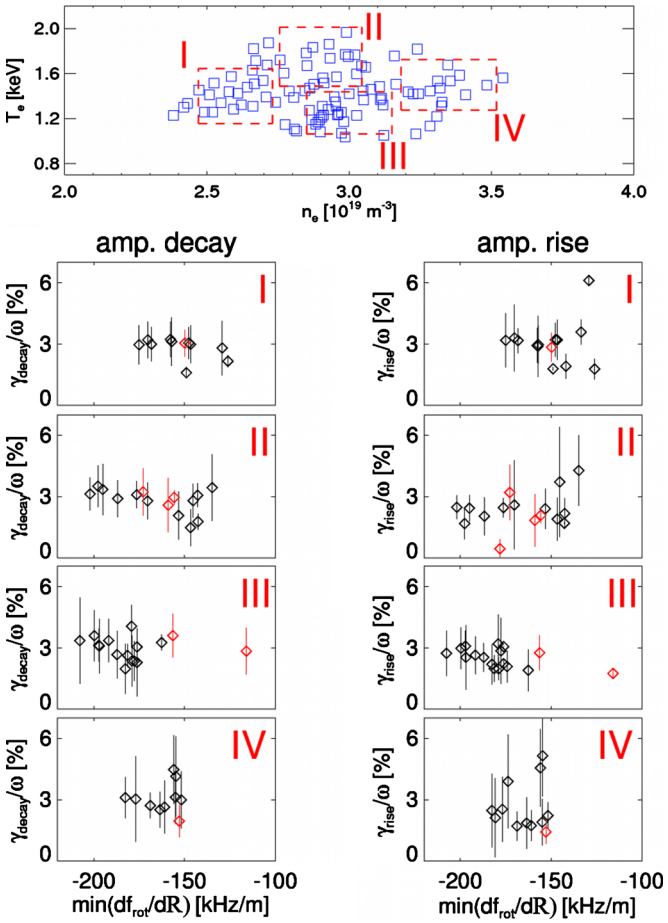

FIG. 10. (Color online) (Top) Parameter space from an ensemble of ten discharges with different NB timings and powers. The bottom panels show the amplitude decay (left column) and rise (right column) rates vs maximum rotation shear for the subsets of density and temperature values indicated in the top panel as regions I to IV. Symbols and vertical bars indicate the average and standard deviation of the measured rates over 10 ms, corresponding to the sampling time of toroidal rotation measurements. Light symbols denote time points with up to 1.5 MW of injected rf power in addition to NB injection.

displace two regions of the mode structure separated by ΔR_{mode} under the effects of a local differential velocity $|\partial(2\pi R f_{\mathrm{rot}})/\partial R|$ calculated at $R=R_{\mathrm{mode}}$,

$$\tau_{\mathrm{dec}}^{-1} \simeq k_{\|}\Delta R_{\mathrm{mode}} 2\pi R_{\mathrm{mode}} \left|\frac{\partial f_{\mathrm{rot}}}{\partial R}\right|_{R=R_{\mathrm{mode}}}, \qquad (2)$$

where $k_{\|}\approx|n-m/q_{\mathrm{min}}|/R_{\mathrm{mode}}$ is the parallel wavenumber, R_{mode} the location of maximum mode amplitude, and ΔR_{mode} the radial extension of the mode. From Fig. 1–6, typical values of $|\partial f_{\mathrm{rot}}/\partial R|$ measured at $R=120-135$ cm, where the TAEs have their maximum amplitude, result in a decorrelation time $\tau_{\mathrm{dec}}\sim 1$ ms. Values $\Delta R_{\mathrm{mode}}=10-20$ cm, derived from reflectometer measurements of the mode structure (Fig. 2), are used. Although these values are roughly consistent with the calculated autocorrelation time for the dominant TAEs, no steep transition in the rotation (or its shear) is observed. Therefore, the decorrelation from sheared rotation alone seems not responsible for the observed mode behavior.

IV. MODE FREQUENCY, CROSS-PHASE, AND AMPLITUDE RISE/DECAY RATES

The NSTX multichannel reflectometer system provides radially localized information on the mode evolution. An eventual shearing off of the mode through differential plasma rotation should therefore appear from correlation analysis of channels measuring across the shear layer. Results for the dominant $n=3$ mode are shown in Fig. 7 for a time window corresponding to two bursts [Fig. 7(a)]. The two channels measure at $R\approx 117$ cm and $R\approx 125$ cm. For each channel, the instantaneous frequency (in the laboratory frame) is reconstructed from the band-pass filtered signals [Fig. 7(b)]. The mode frequency shifts down by ~ 10 kHz over 300 μs with no significant difference as a function of the minor radius (Fig. 8). The frequencies are significantly different only when the signal-to-noise is too low and the analysis fails. This can be seen from the vanishing amplitude and quantified by a sudden drop in the cross-correlation [Figs. 7(a)–7(c)]. Finally, the phase shift between the two channels is shown in Fig. 7(d). No systematic variations of the cross-phase are observed. The invariance of frequency and cross-phase is in contrast with the picture that the mode experiences a differential rotation, which should appear as a Doppler shift contribution to $f_{\mathrm{lab},n}^{\mathrm{TAE}}$ [Eq. (1)] that depends on the radial position.

The analysis of the time scales of the TAE bursts complements the previous conclusions. The mode amplitude evolution during a burst provides insight into the effective

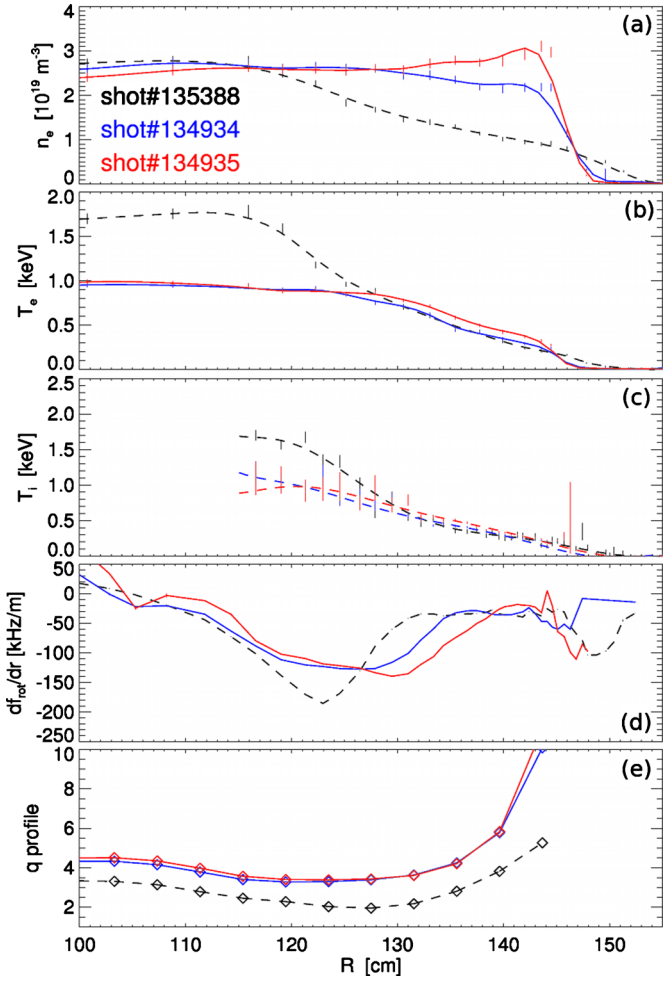

FIG. 11. (Color online) Radial profiles of (a) electron density, (b) electron and (c) ion temperature, (d) toroidal velocity shear, and (e) q profile at $t=310$ ms for the L-mode discharge in Fig. 1 (dotted line, shown here for reference) and for two of the three H-mode discharges with (solid line) and without (dashed line) HHFW injection. Strong TAE activity with similar bursting/chirping features is measured (Fig. 12) except for no-rf discharge.

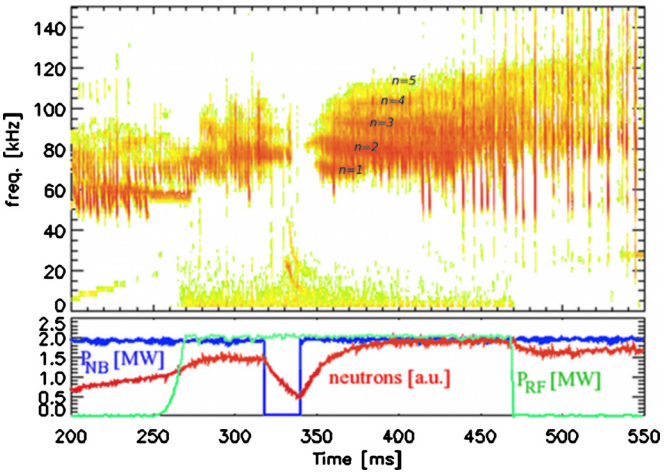

FIG. 12. (Color online) (Top) Spectrogram of TAE activity for discharge 134934. Note the decay of TAE activity during the NB notch, indicating that the fast ion population, hence the drive for the modes, is decreasing, as observed in the neutron rate. (Bottom) Waveforms of injected NB and rf power and measured neutron rate.

rise and decay time for the mode amplitude, γ_{rise} and γ_{decay}. The rising (falling) amplitude is fitted with a increasing (decreasing) exponential to estimate the corresponding time constant. Considering the possible nonlinear dynamics of the modes[4] and the still finite drive and damping at play during both growth and decay phases, these quantities should not be confused with the linear growth and damping rates of the modes. They represent an experimentally accessible estimate of the typical time scales governing the mode evolution. Only in the limit of vanishing damping during the amplitude growth and vanishing drive during its decay the two time constants approximate the linear rates, under the additional assumption of linear or weakly nonlinear dynamic. The normalized ratio of rise/decay rate to the mode frequency can be inferred by dividing γ_{rise} and γ_{decay} by $\omega=2\pi f^{\text{TAE}}_{\text{lab},n}$. Figure 9 shows the results of this analysis by comparing the temporal evolution of the maximum rotation shear, rms mode amplitude (as measured by Mirnov coils), and the estimated $\gamma_{\text{rise}}/\omega$ and $\gamma_{\text{decay}}/\omega$ ratios. Rise and decay terms do not vary in a consistent way with the $>50\%$ increase in the rotation gradient, the dramatic change in the mode amplitude and the overall mode dynamics. The decorrelation rate from Eq. (2), calculated for $n=3$ and poloidal mode number $m=-6\cdots+6$, remains below 1%, i.e., considerably smaller than the estimated γ_{rise} and γ_{decay}. (In this case, the γ/ω ratio is calculated by using the reconstructed frequency in the plasma frame.)

In general, no statistically significant trend of the effective rise and decay rates as a function of the maximum shear is observed. This is illustrated in Fig. 10 for $n=3$ mode activity from a series of similar discharges with varying level of injected NB and rf power. (Similar results are obtained for other modes with different n's.) Since electron density and temperature span a wide range, four subsets are shown separately to group data characterized by similar values ofdamping on the thermal plasma. The role of other damping mechanisms, such as continuum damping, is not considered in this analysis.

V. IMPORTANCE OF TAE DRIVE VERSUS ROTATION SHEAR EFFECTS

The results from the previous sections suggest an alternative interpretation for the bursting TAE behavior observed in NSTX plasmas based on the role of the TAE drive instead of the damping through rotation shear. In fact, the condition $\gamma_{\text{decay}}\approx\gamma_{\text{rise}}$ with both terms large ($>2\%$, according to Figs. 9(c) and 10) reminds the requisite of many models for the appearance of bursting behavior, namely, nearly equal and large drive and damping rates.[30] Although the models are usually one-dimensional and based on a bump-on-tail excitation of the modes, their results can be qualitatively generalized to a more complex case with spatial (instead of velocity) gradient as steady source of free energy, to which kinetic effects resulting from wave-particle interactions add.

Experimentally, two ways are available to modify the drive for TAEs. First, NB sources with different tangency radii can be used. For the shot discussed so far (cf. Fig. 1) the two sources with smaller tangency radius, implying more

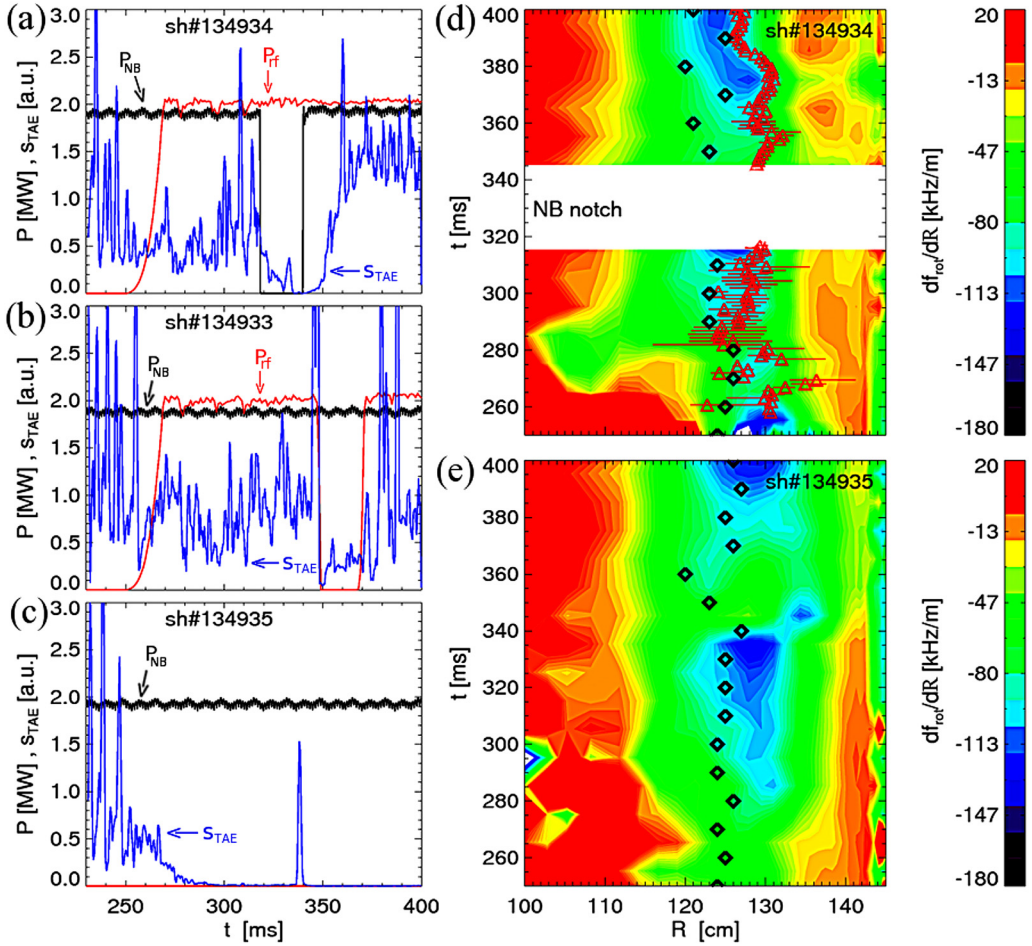

FIG. 13. (Color online) Comparison of rms TAE activity over the frequency band 40–120 kHz (blue) for three discharges with different NB and rf power waveforms. TAE activity is stronger when both auxiliary power sources are ON, whereas NB injection alone is insufficient to sustain the modes. (a) $P_{NB} \approx P_{rf} \approx 2$ MW, with a notch in P_{NB}. (b) $P_{NB} \approx P_{rf} \approx 2$ MW, with a notch in P_{rf}. (c) $P_{NB} \approx 2$ MW and $P_{rf}=0$. [(d) and (e)] Same as in Fig. 6 for discharges 134934 (with rf) and 134935 (no rf and no measurable TAE activity). Note that no rotation data are available during the NB notch for discharge 134934. The spike in the Mirnov coils' signal occurring at 330–340 ms in frames (b) and (c) is due to transient MHD activity with frequency up to 50 kHz.

perpendicular injection, were used. In the following, the source at tangency radius of 69 cm is utilized, providing more tangential injection and the possibility of direct measurements of the q-profile through motional Stark effect.[31] Second, rf injection can be used to affect the evolution of the fast ion and rotation profiles,[13,32] both ultimately dependent on the beam deposition profile in NB-only discharges. rf waves modify the original beam distribution by scattering and accelerating fast ions. The effect is especially important in a spherical tokamak such as NSTX where numerous resonances are simultaneously present over the entire minor radius.[33]

Three shots with different timing of NB and rf injection are compared. Apart from the auxiliary power the plasma profiles are qualitatively similar for these discharges, at least in the initial ≈ 350 ms (Fig. 11). Electron temperature and q profiles are nearly identical. The density profiles match well inside $R=135$ cm, whereas a difference of $\sim 30\%$ is observed closer to the edge. The profile and value of rotation shear are also qualitatively comparable. Unlike the L-mode discharge of Fig. 1, whose profiles are also shown in Fig. 11 for reference, plasmas transition into H-mode. Reflectometer data are therefore not available because of the flat density profile inside $R \sim 140$ cm. The first discharge has $P_{NB}=2$ MW with a beam notch (i.e., zero power) at 320–340 ms, see Figs. 12 and 13(a). The injected rf power is constant at $P_{rf}=2$ MW from $t \approx 260$ ms on. In spite of the different conditions with respect to the L-mode scenario described earlier (Fig. 1), activity in the Alfvén band is similar, with RSAEs shifting into TAEs at the beginning of the current flat-top. A bursting phase precedes a phase with larger mode activity, during which avalanches eventually occur (Fig. 12). TAE activity decays during the beam notch, then increases again as the beam turns back on, consistent with the fact that the injected fast ions are the primary drive for TAEs. A slight decrease in rotation shear is observed [Fig. 13(d)] during the beam notch, then the rotation recovers to the previous values in $\lesssim 20$ ms. The second discharge is similar, but with constant P_{NB} and a notch in P_{rf} at 350–370 ms [Fig. 13(b)]. TAE activity decreases during the notch, where only small bursts are observed until the rf is turned back on and the mode amplitude is restored to a level comparable to that before the notch. In the third discharge the injected rf power is zero. RSAEs are observed during the

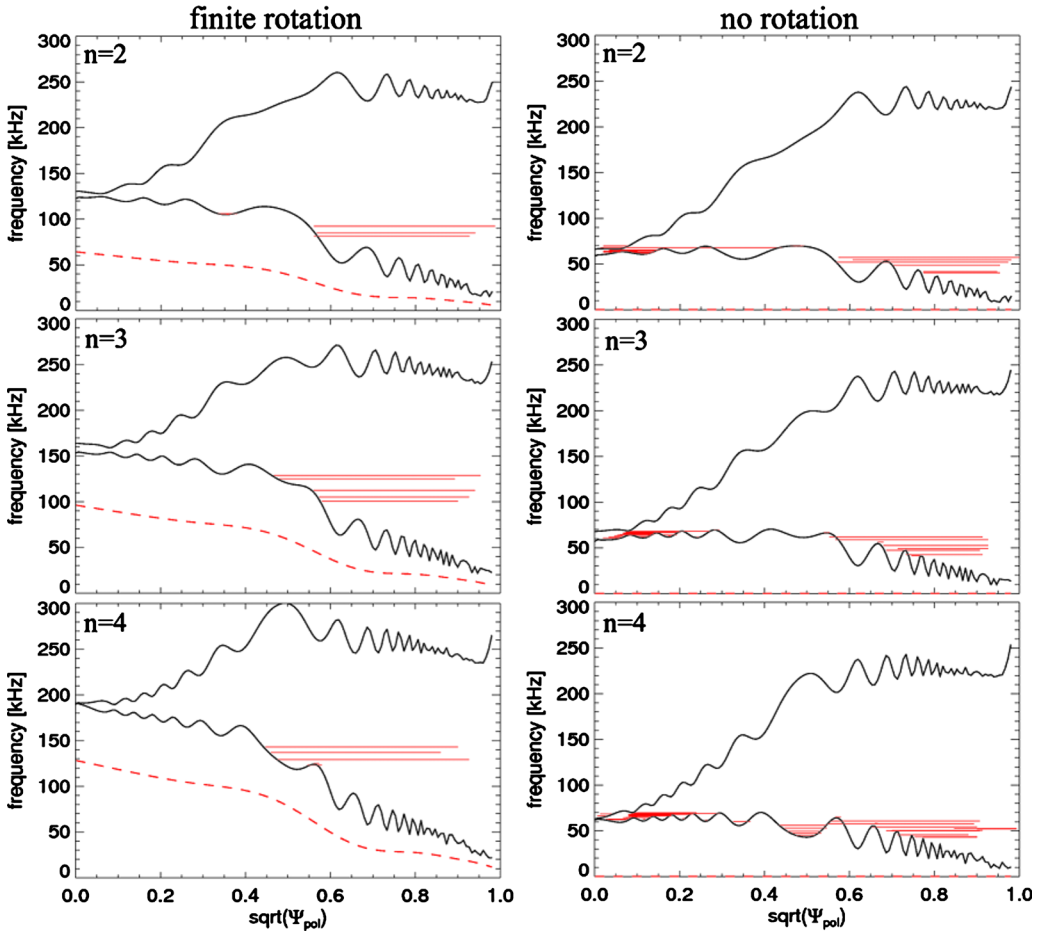

FIG. 14. (Color online) TAE continuum and frequency of the ideal $n=2,3,4$ eigenmodes (horizontal lines) calculated through NOVA-K for discharge 135388 at $t=280$ ms. The mode frequency calculation is limited to the range corresponding to the experimentally measured modes. Plasma profiles assuming finite (left column) and zero rotation (right column) are used as input for NOVA-K. The dashed line in the left column represents the Doppler shift frequency term nf_{rot} calculated from the measured profile of toroidal rotation.

ramp-up phase, but they decay after $t \approx 270$ ms. No TAEs are measured afterwards [Figs. 13(c) and 13(e)]. These observations are explained by assuming that a threshold in the fast ion population has not been crossed[9] compared to the discharge in Fig. 1, and NB-only injection is not sufficient to destabilize TAEs. When rf is applied, acceleration of fast ions partly compensates the Coulomb drag and their distribution function is modified,[33] making the drive for TAEs stronger. However, rf alone is not enough to sustain the fast ion population and TAEs decay when the NB is switched off as in Fig. 13(a). All these considerations point to the fast ion drive as primary cause for the observed TAE dynamics, with rotation shear playing only a marginal role.

VI. SUMMARY AND CONCLUSIONS

The role of a shear layer in the toroidal rotation profile on the dynamics of TAE modes has been studied in L- and H-mode discharges on NSTX. Toroidal rotation is driven by NB injection, which also represents the source term for the fast ion population. This determines a coupling between the spatial location of the shear layer and of the TAE drive. H-mode discharges with simultaneous NB and rf injection are partially successful in decoupling the two terms, but no strong modifications of the TAE behavior are observed. Results from a multichannel reflectometer system measuring TAE fluctuations across the shear layer indicate that the modes rotate rigidly. Within the experimental uncertainties, no evidence of spatial decorrelation on the frequency and phase shift evolution caused by the velocity gradient is observed. This indicates that for the scenarios investigated in this work, sheared rotation is much less efficient in decorrelating global, coherent modes as TAEs as compared to other turbulent instabilities, for which sheared flows provide an effective suppression mechanism.[34,35] The experimental results lead to consider the TAE drive term, rather than the decorrelation from rotation shear, as the primary cause for the observed bursting dynamics of the modes. Experiments aimed at altering the TAE drive, both in real space (through variations of the tangency radius of the NB source) and in velocity space (by applying rf heating), are consistent with this conclusion. These observations differ from those reported in Refs. 11–13, but the very different experimental scenarios discussed herein, as mentioned in Sec. I, must be considered before attempting any direct comparison. Further studies, possibly assisted by the predictions of numerical codes, would be required to assess quantitatively the depen-

dence of TAE dynamic on aspect ratio, q profile, and instability drive for the different scenarios. Such effort is clearly beyond the scope of this work.

Apart from the shear in rotation, it is important to point out that the rotation profile itself can strongly modify the structure of the Alfvén continuum.[18,17] As a consequence, the stability of TAE modes may also change with rotation. In order to exemplify the possible effects of rotation on structure and stability of TAEs and on the interpretation of experiments through numerical codes, an example based on the NOVA-K code[36] is illustrated in Fig. 14. The reference discharge is the same shown in Fig. 1 at $t=280$ ms, i.e., just before the beginning of the bursting/chirping phase. It is seen that the continuum is modified by the f_{rot} profile, which in turn leads to different (ideal) eigenmodes with varying radial extension and mode structure.[9] Depending on their proximity to the continuum, modes inside the TAE gap may experience a strong continuum damping or not. Because of the large rotation frequency and magnetic shear typical of low aspect ratio plasmas, the impact of the details of the f_{rot} profile on TAE stability can be expected to be more important in NSTX than in conventional devices. It should be noted that in this calculation the finite rotation is accounted for as a simple Doppler shift of the calculated gap frequencies;[37] it is not included self-consistently in the computation of the continuum structure. An extensive discussion of the dependence of NOVA-K predictions upon input parameters such as rotation and q profile can be found in Ref. 9 and is not repeated here.

A closer comparison with numerical codes would be required for more detailed investigations. A version of NOVA-K including a more complete treatment of finite plasma rotation is being developed and will be used in future studies. Other codes, such as the nonlinear, self-consistent code M3D-K (Ref. 38 and references therein) already include toroidal rotation. Initial results indicate that modifications of the TAE gap structure for different rotation profiles are more important for TAE dynamics than the rotation shear,[17] which is consistent with the results presented herein. Regarding stability calculations for TAEs, a correct quantitative treatment of continuum damping, including, for instance, kinetic effects, is still missing in the numerical codes. It would be required for quantitative comparisons of calculated mode stability against experiments. At the same time good progress has been made in the past few years to understand and model the interaction between fast ions and rf.[24,33,39] Integrating those tools in codes such as TRANSP,[40] in order to make analysis of rf discharges routinely available, is still work in progress. It may provide a powerful tool to investigate TAE dynamics on a quantitative basis.

Future experiments on NSTX will further investigate the role of rotation and drive in the TAE dynamics. Improved characterization of the mode structure is expected through beam emission spectroscopy.[41] A second FIDA system, more sensitive to the tangential component of the fast ion distribution function, will provide more details on the fast ion dynamic.[42] In addition, the possibility of using magnetic braking[43] to alter the rotation profile independently of the NB torque source will be explored.

ACKNOWLEDGMENTS

Discussions with Dr. G.-Y. Fu and the support of the NSTX NB and RF groups are gratefully acknowledged. This work is supported by U.S.-DOE Grant No. DE-FG02-06ER54867 and by U.S. DOE Contract Nos. DE-AC02-09CH11466 and DE-FG02-99ER54527.

[1] A. Fasoli, C. Gormezano, H. L. Berk, B. N. Breizman, S. Briguglio, D. S. Darrow, N. N. Gorelenkov, W. W. Heidbrink, A. Jaun, S. V. Konovalov, R. Nazikian, J.-M. Noterdaeme, S. Sharapov, K. Shinoara, D. Testa, K. Tobita, Y. Todo, G. Vlad, and F. Zonca, Nucl. Fusion **47**, S264 (2007).
[2] W. W. Heidbrink, Phys. Plasmas **15**, 055501 (2008).
[3] B. V. Chirikov, Phys. Rep. **52**, 263 (1979).
[4] H. L. Berk, B. N. Breizman, and M. S. Pekker, Phys. Plasmas **2**, 3007 (1995).
[5] A. Fasoli, B. N. Breizman, D. Borba, R. F. Heeter, M. S. Pekker, and S. E. Sharapov, Phys. Rev. Lett. **81**, 5564 (1998).
[6] M. P. Gryaznevich and S. E. Sharapov, Plasma Phys. Controlled Fusion **46**, S15 (2004).
[7] S. S. Medley, N. N. Gorelenkov, R. Andre, R. E. Bell, D. S. Darrow, E. D. Fredrickson, S. M. Kaye, B. P. LeBlanc, A. L. Roquemore, and NSTX Team, Nucl. Fusion **44**, 1158 (2004).
[8] M. Podestà, W. W. Heidbrink, D. Liu, E. Ruskov, R. E. Bell, D. S. Darrow, E. D. Fredrickson, N. N. Gorelenkov, G. J. Kramer, B. P. LeBlanc, S. S. Medley, A. L. Roquemore, N. A. Crocker, S. Kubota, and H. Yuh, Phys. Plasmas **16**, 056104 (2009).
[9] E. D. Fredrickson, N. A. Crocker, R. E. Bell, D. S. Darrow, N. N. Gorelenkov, G. J. Kramer, S. Kubota, F. M. Levinton, D. Liu, S. S. Medley, M. Podestà, K. Tritz, R. B. White, and H. Yuh, Phys. Plasmas **16**, 122505 (2009).
[10] M. Ono, S. M. Kaye, Y.-K. M. Peng, G. Barnes, W. Blanchard, M. D. Carter, J. Chrzanowski, L. Dudek, R. Ewig, D. Gates, R. E. Hatcher, T. Jarboe, S. C. Jardin, D. Johnson, R. Kaita, M. Kalish, C. E. Kessel, H. Kugel, R. Maingi, R. Majeski, J. Manickam, B. McCormack, J. Menard, D. Mueller, B. Nelson, B. Nelson, C. Neumeyer, G. Oliaro, F. Paoletti, R. Parsells, E. Perry, N. Pomphrey, S. Ramakrishnan, R. Raman, G. Rewoldt, J. Robinson, A. L. Roquemore, P. Ryan, S. Sabbagh, D. Swain, E. J. Synakowski, M. Viola, M. Williams, J. R. Wilson, and NSTX Team, Nucl. Fusion **40**, 557 (2000).
[11] D. Testa, C. Boswell, A. Fasoli, and JET-EFDA Contributors, Nucl. Fusion **45**, 907 (2005).
[12] A. Fasoli, D. Borba, G. Bosia, D. J. Campbell, J. A. Dobbing, C. Gormezano, J. Jacquinot, P. Lavanchy, J. B. Lister, P. Marmillod, J.-M. Moret, A. Santagiustina, and S. Sharapov, Phys. Rev. Lett. **75**, 645 (1995).
[13] M. Saigusa, Y. Kusama, T. Ozeki, H. Kimura, T. Fujita, S. Moriyama, T. Fujii, M. Azumi, V. I. Afanassiev, and Y. Neyatani, Nucl. Fusion **37**, 1559 (1997).
[14] D. A. Spong, B. A. Carreras, and C. L. Hedrick, Phys. Plasmas **1**, 1503 (1994).
[15] S. C. Jardin, C. E. Kessel, J. Menard, T. K. Mau, R. Miller, F. Najmabadi, V. S. Chan, L. L. Lao, Y. R. Linliu, R. L. Miller, T. Petrie, P. A. Politzer, and A. D. Turnbull, Fusion Eng. Des. **65**, 165 (2003).
[16] Y.-K. M. Peng, P. J. Fogarty, T. W. Burgess, D. J. Strickler, B. E. Nelson, J. Tsai, C. A. Neumeyer, R. E. Bell, C. Kessel, J. Menard, D. Gates, B. P. LeBlanc, D. Mikkelsen, E. Fredrickson, L. Grisham, J. Schmidt, P. Rutherford, S. A. Sabbagh, A. Field, A. Sykes, I. Cook, O. Mitarai, and Y. Takase, Plasma Phys. Controlled Fusion **47**, B263 (2005).
[17] G. Y. Fu, private communication (2010).
[18] B. van der Holst, A. J. C. Belien, and J. P. Goedbloed, Phys. Plasmas **7**, 4208 (2000).
[19] E. D. Fredrickson, N. N. Gorelenkov, R. E. Bell, J. E. Menard, A. L. Roquemore, S. Kubota, N. A. Crocker, and W. Peebles, Nucl. Fusion **46**, S926 (2006).
[20] B. P. LeBlanc, Rev. Sci. Instrum. **79**, 10E737 (2008).
[21] R. E. Bell, R. Andre, S. M. Kaye, R. A. Kolesnikov, B. P. LeBlanc, G. Rewoldt, W. X. Wang, and S. A. Sabbagh, Phys. Plasmas **17**, 082507 (2010).
[22] Y. B. Kim, P. H. Diamond, and R. J. Groebner, Phys. Fluids B **3**, 2050 (1991).
[23] S. M. Kaye, W. Solomon, R. E. Bell, B. P. LeBlanc, F. Levinton, J. E.

Menard, G. Rewoldt, S. Sabbagh, W. Wang, and H. Yuh, Nucl. Fusion **49**, 045010 (2009).
[24]G. Taylor, R. E. Bell, J. C. Hosea, B. P. LeBlanc, C. K. Phillips, M. Podestà, E. J. Valeo, J. R. Wilson, J.-W. Ahn, G. Chen, D. L. Green, E. F. Jaeger, R. Maingi, P. M. Ryan, J. B. Wilgen, W. W. Heidbrink, D. Liu, P. T. Bonoli, T. Brecht, M. Choi, and R. W. Harvey, Phys. Plasmas **17**, 056114 (2010).
[25]N. A. Crocker, E. D. Fredrickson, N. N. Gorelenkov, G. J. Kramer, D. S. Darrow, W. W. Heidbrink, S. Kubota, F. M. Levinton, H. Yuh, J. E. Menard, B. P. LeBlanc, and R. E. Bell, Phys. Plasmas **15**, 102502 (2008).
[26]J. E. Menard, private communication (2008).
[27]N. P. Young, S. E. Sharapov, V. M. Nakariakov, and JET EFDA Contributors, Plasma Phys. Controlled Fusion **48**, 295 (2006).
[28]E. J. Strait, W. W. Heidbrink, and A. D. Turnbull, Plasma Phys. Controlled Fusion **36**, 1211 (1994).
[29]M. Podestà, W. W. Heidbrink, R. E. Bell, and R. Feder, Rev. Sci. Instrum. **78**, 10E521 (2008).
[30]H. L. Berk, B. N. Breizman, J. Fitzpatrick, M. S. Pekker, H. V. Wong, and K. L. Wong, Phys. Plasmas **3**, 1827 (1996).
[31]F. M. Levinton, R. J. Fonck, G. M. Gammel, R. Kaita, H. W. Kugel, E. T. Powell, and D. W. Roberts, Phys. Rev. Lett. **63**, 2060 (1989).
[32]D. Borba, G. D. Conway, S. Guenter, G. T. A. Huysmans, S. Klose, M. Maraschek, A. Mueck, I. Nunes, S. D. Pinches, and F. Serra, and ASDEX Upgrade Team, Plasma Phys. Controlled Fusion **46**, 809 (2004).
[33]D. Liu, W. W. Heidbrink, M. Podestà, R. E. Bell, E. D. Fredrickson, S. S. Medley, R. W. Harvey, and E. Ruskov, Plasma Phys. Controlled Fusion **52**, 025006 (2010).
[34]K. H. Burrell, Phys. Plasmas **4**, 1499 (1997).
[35]P. W. Terry, Rev. Mod. Phys. **72**, 109 (2000).
[36]C. Z. Cheng, Phys. Rep. **211**, 1 (1992).
[37]G. J. Kramer, R. Nazikian, B. Alper, M. de Baar, H. L. Berk, G.-Y. Fu, N. N. Gorelenkov, G. McKee, S. D. Pinches, T. L. Rhodes, S. E. Sharapov, W. M. Solomon, M. A. van Zeeland, and JET EFDA Contributors, Phys. Plasmas **13**, 056104 (2006).
[38]W. Park, E. V. Belova, G. Y. Fu, X. Z. Tang, H. R. Strauss, and L. E. Sugiyama, Phys. Plasmas **6**, 1796 (1999).
[39]M. Choi, D. Green, W. W. Heidbrink, R. W. Harvey, D. Liu, V. S. Chan, L. A. Berry, F. Jaeger, L. L. Lao, R. I. Pinsker, M. Podestà, D. N. Smithe, J. M. Park, and P. T. Bonoli, Phys. Plasmas **17**, 056102 (2010).
[40]R. V. Budny, Nucl. Fusion **34**, 1247 (1994).
[41]D. R. Smith, H. Feder, R. Feder, R. J. Fonck, G. Labik, G. R. McKee, N. Schoenbeck, B. Stratton, I. Uzun-Kaymak, and G. Winz, Rev. Sci. Instrum. **81**, 10D718 (2010).
[42]A. Bortolon, W. W. Heidbrink, and M. Podestà, Rev. Sci. Instrum. **81**, 10D728 (2010).
[43]W. Zhu, S. A. Sabbagh, R. E. Bell, J. M. Bialek, M. G. Bell, B. P. LeBlanc, S. M. Kaye, F. M. Levinton, J. E. Menard, K. C. Shaing, A. C. Sontag, and H. Yuh, Phys. Rev. Lett. **96**, 225002 (2006).